J. Membrane Biol. 15, 159–192 (1974)

Shape of the Hydrophobic Barrier of Phospholipid Bilayers (Evidence for Water Penetration in Biological Membranes)

O. H. Griffith, P. J. Dehlinger and S. P. Van

Institute of Molecular Biology and Department of Chemistry,
University of Oregon, Eugene, Oregon 97403

Received 9 July 1973; revised 21 September 1973

Summary. Previous work has shown that there is a small solvent effect on the electron spin resonance spectra of nitroxide spin labels. The aim of this paper is to develop a semiquantitative treatment of the solvent effects and to use this treatment to estimate the shape of the hydrophobic barrier (i.e., polarity profile) of lipid bilayers.

In this semiquantitative treatment of solvent effects, the total effect on the isotropic ^{14}N coupling constant, AA, is expressed as a sum of terms associated with van der Waals interactions, hydrogen bonding, the charged double layer of phospholipid polar groups and the membrane potential. The magnitude of AA as a function of the electric field is estimated with Hückel molecular orbital theory and, independently, using the Onsager model. With these relations, estimates of the relative importance of the various solvent effect terms are obtained from accurate ESR measurements on dilute solutions of di-*t*-butyl nitroxide in thirty-three solvents and calculations of the electric field produced by the charged double layer and the membrane potential.

To estimate the shape of the hydrophobic barrier of lipid bilayers, fatty acids and L-α-lecithins with doxyl (i.e., 4′,4′-dimethyloxazolidine-N-oxyl) labels bonded to various positions along the lipid chains were diffused into phospholipid vesicles and membranes (from the calf liver microsomal fraction). The shape of the hydrophobic barrier is plotted as a polarity index operationally defined in terms of the AA of the lipid spin labels. The effect of the charged double layers is less important than water penetration except when the spin label is within a few Angstroms of the charged groups. Any effects of a membrane potential on AA are insignificant. A comparison of ESR spectra indicates that significant water penetration into the bilayer occurs in both the pure lipid bilayers and in the membrane preparations.

The existence of a lipoid barrier in biological membranes was recognized in the earliest permeability studies (Davson & Danielli, 1943). The early work combined with extensive recent studies provides convincing evidence that phospholipid bilayers do exist in a variety of biological membranes, and serve not only as a barrier to indiscriminate ion transport but as a two-dimensional fluid with solvent properties affecting the organization and distribution of membrane proteins (for reviews *see* Jost, Waggoner & Griffith, 1971*b*; Singer, 1971; Steck, Fairbanks & Wallach, 1971; Vanderkooi & Green, 1971; Branton & Deamer, 1972; Singer & Nicolson, 1972). It is of

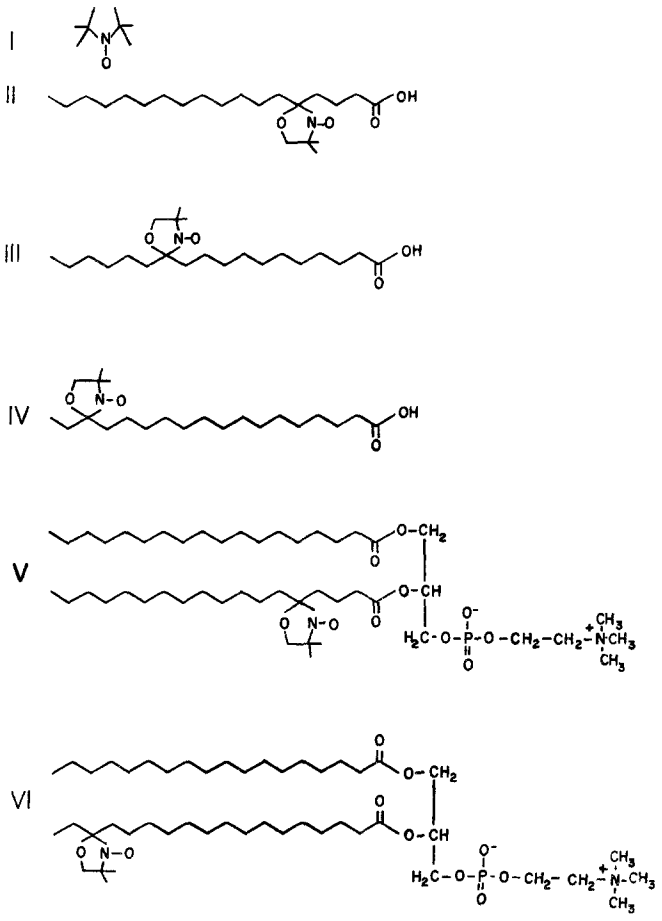

Fig. 1. Spin labels used in this study: di-*t*-butyl nitroxide (I); 5-, 12- and 16-doxylstearic acids (II–IV); and typical components of the spin-labeled L-α-lecithins (V, VI)

interest to measure the shape of this hydrophobic barrier in the direction normal to the bilayer surface. In principle, spin labeling provides one approach. A small solvent dependence on the electron spin resonance (ESR) parameters was reported some time ago (Briere, Lemaire & Rassat, 1965) and several investigators have noted a solvent effect in spin label studies of membrane model systems, liquid crystals and biological membranes (Waggoner, Griffith & Christensen, 1967; Waggoner, Keith & Griffith, 1968; Hubbell & McConnell, 1968, 1971; Seelig, 1970; Griffith, Libertini & Birrell, 1971; Jost, Libertini, Hebert & Griffith, 1971*a*; Seelig, Limacher & Bader, 1972). Most of these studies have measured, either directly or indirectly, small variations in the isotropic splitting constant (A_0) or *g*-value (g_0) of small rapidly tumbling spin labels such as I in Fig. 1, or of several of the positional isomers of the doxyl lipid spin labels (e.g. II–VI).

The ESR line shapes of lipid spin labels in lipid vesicles and membranes are frequently broad, and it is difficult to obtain ESR parameters with sufficient accuracy to examine any small solvent shifts. In spite of these difficulties the lipid spin labels (e.g., fatty acids, phospholipids, etc.) with doxyl groups bonded at different positions along the chains represent one of the few methods of obtaining the desired polarity data. For this reason we report here a semiquantitative treatment of solvent perturbations based on a systematic study of both types of spin labels I and II–IV in homogeneous solvents. We apply the treatment to membranes of the microsomal fraction and to the corresponding lipid vesicles, and arrive at an approximate shape of the hydrophobic barrier for this system. We then examine the generality of the results using a more limited set of data on myelin and myelin lipid vesicles.

Experimental

Di-*t*-butyl nitroxide (I) was obtained from Eastman Organic Chemicals. The three positional isomers of doxylstearic acid (II–IV) are the same spin labels prepared previously (Waggoner, Kingzett, Rottschaefer, Griffith & Keith, 1969; Jost *et al.*, 1971*a*) but are now purchased from Syva Associates. Positional isomers of spin-labeled lecithin (V, VI) were generously provided by Messrs. T. Marriott and T. Micka, and had been prepared by coupling the corresponding doxylstearic acids to egg lysolecithin by published methods (Selinger & Lapidot, 1966; Hubbell & McConnell, 1971). The solvents used to obtain the solvent dependence of A_0 and g_0 for I were of reagent or spectral quality, and all reagent grade solvents except diethyl ether were freshly distilled before use.

Microsomes were isolated from calf liver by standard procedures (Omura, Siekevitz & Palade, 1967) and washed with 0.1 M potassium phosphate buffer, pH 6.5. Myelin was prepared from the white matter of fresh beef brain after the method of Eichberg, Whittaker and Dawson (1964) and washed with 0.1 M potassium phosphate buffer, pH 6.5. Total lipids were extracted from the membrane preparations by the method of Folch, Lees and Stanley (1957). The lipids were dried under vacuum, dissolved in chloroform, and stored at -18 °C under nitrogen. Aqueous dispersions of lipid vesicles containing lipid spin labels were prepared by mixing 10 mg of lipid sample and 0.05 mg of II–IV or 0.10 mg of V or VI in chloroform, evaporating the solvent with nitrogen gas, then sonicating the mixture in 1 ml of 0.1 M potassium phosphate buffer, pH 6.5, for 2 min on ice. Doxylstearic acid spin labels were introduced into the biological membrane preparations by sonicating 1 ml of suspended membrane sample (10 mg protein/ml of 0.1 M potassium phosphate buffer, pH 6.5) and 0.05 mg spin label for 2 min on ice. The lipid and membrane samples were added to quartz ESR tubes and deoxygenated with nitrogen gas. Lipid samples containing I, on which 35 GHz ESR measurements were made, were prepared by drying under nitrogen gas about 3 mg of lipid in a small conical centrifuge tube and adding to this 25 lambda of 3×10^{-4} M I in 0.1 M potassium phosphate buffer, pH 6.5. After thorough mixing with a glass rod, the lipid pastes were drawn into 0.4 mm (I.D.) capillary tubes which then were sealed at both ends with red wax. The biomembrane samples containing I were prepared by adding the membrane sample (containing 10 mg protein) to 2 ml of 3×10^{-4} M I in 0.1 M potassium phosphate buffer, pH 6.5, and homogenizing briefly. The suspension was centrifuged at $105{,}000\times g$ for 1 hr, and the membrane pellet forced into a 0.4 mm capillary tube and sealed.

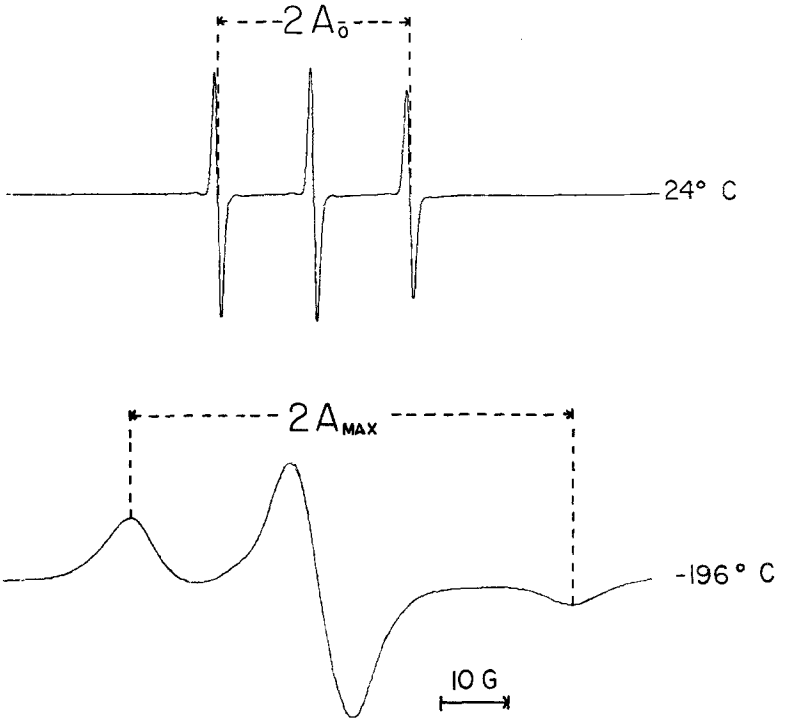

Fig. 2. 9.5 GHz ESR spectra of 16-doxylstearic acid in ethanol at sample temperatures of 24 and −196 °C. The spectra illustrate the method used in measuring A_0 and A_{max}

Solutions of II–IV in various solvents were prepared by adding 1 ml of solvent to 0.05 mg of spin label and vortexing briefly. Small portions of the solutions were added to capillary tubes and deoxygenated under nitrogen for room temperature ESR spectra. The remainder of the solutions were added to ESR quartz tubes, deoxygenated under vacuum, and frozen in liquid nitrogen. A Varian V-4546 insert dewar was used for samples at liquid nitrogen temperature. For the hydration-dehydration experiments, 10 mg of lipid and 0.05 mg of II–IV or 0.1 mg of V or VI in chloroform were mixed, the solvent evaporated with nitrogen gas, and then 1 ml of distilled water was added and the mixture sonicated for 2 min on ice. The lipid dispersion was dried on a glass slide, smeared onto glass wool, and equilibrated for 24 hr in large closed chambers exposed to either distilled water or phosphorous pentoxide. The glass wool was then loosely inserted in a quartz ESR tube. The tube containing the sample at 100% relative humidity was placed over a vial containing distilled water and equilibrated for 12 hr and sealed. The tube containing the dehydrated sample was evacuated over phosphorous pentoxide and then sealed while still under vacuum.

The ESR spectra were obtained on a Varian E-3 spectrometer or a Varian V4502 spectrometer equipped with either a 9.5 GHz klystron and rectangular dual cavity or a 35 GHz klystron and cylindrical cavity. All coupling constant and g-value data were measured relative to 5×10^{-4} M di-*t*-butyl nitroxide in 0.01 M aqueous phosphate buffer, pH 7.0, made by mixing 14.0 ml of 0.02 M KH_2PO_4, 24.0 ml of 0.01 M Na_2HPO_4 and 62 ml water (Perrin, 1963). In this aqueous solution at 24 °C, the parameters of di-*t*-butyl nitroxide are $A_0=17.16\pm0.01$, measured as in Fig. 2, and $g_0=2.0056\pm0.0001$ (Birrell, Van & Griffith, 1973).

Results

Solvent Dependence of Di-t-butyl Nitroxide ESR Data

The ESR spectral parameters of di-*t*-butyl nitroxide dissolved in thirty-three solvents are listed in Table 1. All data were measured at room tem-

Table 1. Isotropic ESR parameters [a] for di-*t*-butyl nitroxide

No.	Solvent	A_0	g_0
1.	Hexane	15.10	2.0061
2.	Heptane-pentane (1:1) [b]	15.13	2.0061
3.	2-Hexene	15.17	2.0061
4.	1,5-Hexadiene	15.30	2.0061
5.	Di-*n*-propylamine	15.32	2.0061
6.	Piperidine	15.40	2.0061
7.	*n*-Butylamine	15.41	2.0060
8.	Methyl propionate	15.45	2.0061
9.	Ethyl acetate	15.45	2.0061
10.	Isopropylamine	15.45	2.0060
11.	2-Butanone	15.49	2.0060
12.	Acetone	15.52	2.0061
13.	Ethyl acetate saturated with water	15.59	2.0060
14.	N,N-Dimethyl formamide	15.63	2.0060
15.	EPA [c] (5:5:2) [b]	15.63	2.0060
16.	Acetonitrile	15.68	2.0060
17.	Dimethyl sulfoxide	15.74	2.0059
18.	N-Methyl propionamide	15.76	2.0059
19.	2-Methyl-2-butanol	15.78	2.0059
20.	EPA [c] (5:5:10) [b]	15.87	2.0060
21.	1-Decanol	15.87	2.0059
22.	1-Octanol	15.89	2.0059
23.	N-Methyl formamide	15.91	2.0059
24.	2-Propanol	15.94	2.0059
25.	1-Hexanol	15.97	2.0059
26.	1-Propanol	16.05	2.0059
27.	Ethanol	16.06	2.0059
28.	Methanol	16.21	2.0058
29.	Formamide	16.33	2.0058
30.	1,2-Ethanediol	16.40	2.0058
31.	Ethanol/water (1:1) [b]	16.69	2.0057
32.	Water	17.16	2.0056
33.	10 M LiCl aqueous solution	17.52	2.0056

[a] All data measured at room temperature (23 to 24 °C). Estimated uncertainties are ± 0.02 G and ± 0.0001 for A_0 and g_0, respectively, relative to the standard dilute aqueous solution of di-*t*-butyl nitroxide for which $A_0 = 17.16$ G and $g_0 = 2.0056$.

[b] By volume.

[c] EPA designates a mixture of *e*thyl ether (diethyl ether), iso*p*entane (2-methylbutane) and *a*lcohol (ethanol).

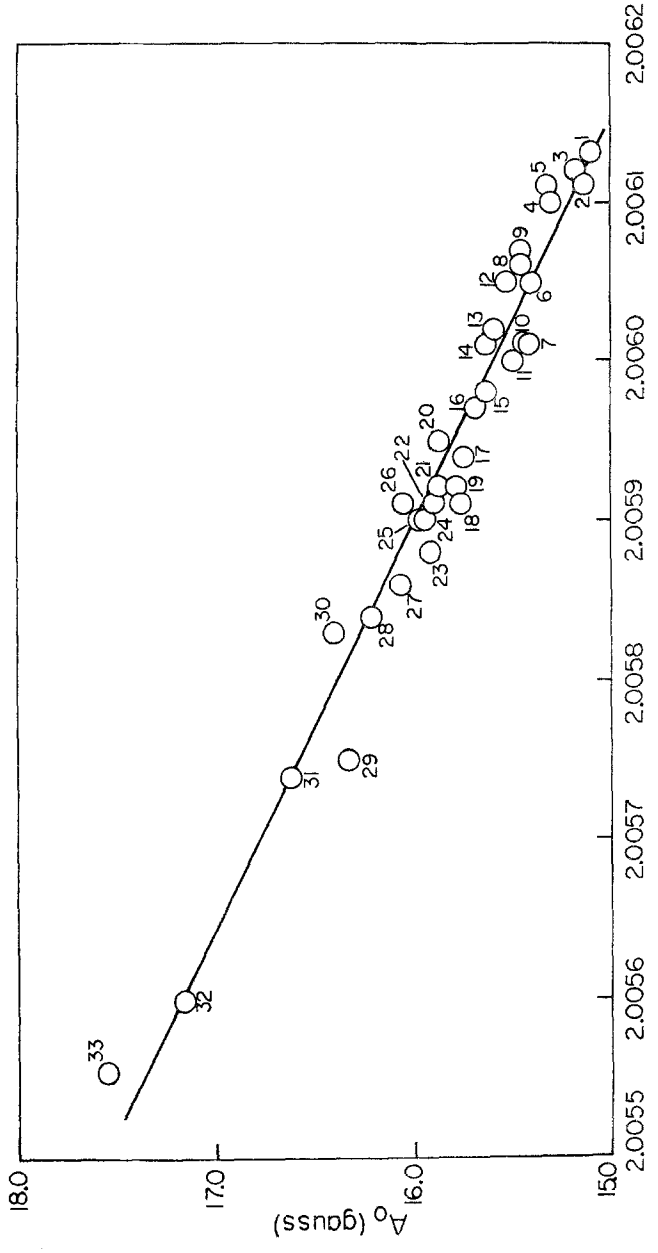

Fig. 3. Solvent dependence of A_0 and g_0 parameters of di-*t*-butyl nitroxide. The data and numbers correspond to Table 1

perature using a 9.5 GHz dual sample cavity and a buffered dilute aqueous di-*t*-butyl nitroxide sample as the reference. The purpose of obtaining these data was to accurately determine the behavior of a simple nitroxide-free radical in different homogeneous environments. Kawamura, Matsunami and Yonezawa (1967) have previously recorded solvent effects on di-*t*-butyl nitroxide. From a plot of A_0 *vs.* g_0, these authors concluded that the data points fall on two lines. One line represents the behavior in aprotic solvents (hexane, carbon tetrachloride, toluene, acetone and acetonitrile) and the second line represents the protic solvents examined (water and methanol). In contrast, the data points of Table 1, which are plotted in Fig. 3, may be described by a single line. There is, however, general agreement between the *relative* shifts in A_0 and g_0 values reported here and the earlier results of Kawamura *et al.* (1967).

Solvent Dependence of Lipid Spin Label ESR Data

In general, obtaining accurate A_0 values of lipid spin labels in randomly oriented phospholipid vesicles or biomembranes is difficult because of the intermediate degrees of molecular motion occurring at room temperature. For this reason, we have employed another solvent-dependent ESR parameter A_{max} as a measure of the polarity sensed by spin labels I–III in lipids and membranes. The quantity A_{max} is measured from spectra of the frozen samples as illustrated in Fig. 2. In the present section we compare the solvent dependence of A_0 and A_{max} for two reasons: (1) to provide a set of values of A_{max} for homogeneous solvents to compare with corresponding values of lipid spin labels in membranes and (2) to construct the standard curve relating A_{max} to A_0, needed to convert all data to one polarity index.

The ESR parameters A_0 and A_{max} were determined at 24 and -196 °C, respectively, for doxylstearic acid spin labels (or methyl esters) in a variety of solvents ranging from ethanol/water to hydrocarbons. In each homogeneous solvent system, the 5-, 12- and 16-doxylstearic acid derivatives yielded very nearly the same A_0 and A_{max} within experimental error. The estimated uncertainties in all A_{max} and A_0 values are ± 0.4 gauss (G) and ± 0.05 G, respectively, as shown by the horizontal and vertical error bars in Fig. 4. The reference line or standard curve of Fig. 4 is a visual fit to these data points for ethanol/water (1:1), ethanol, EPA (5:5:10), EPA (5:5:2), diethyl ether, pentane/heptane (1:1) and mineral oil. These particular solvents were chosen for their solubility characteristics and to enhance formation of rigid glasses rather than microcrystalline solids. Solvents that readily crystallize frequently exclude the spin labels, effectively increasing

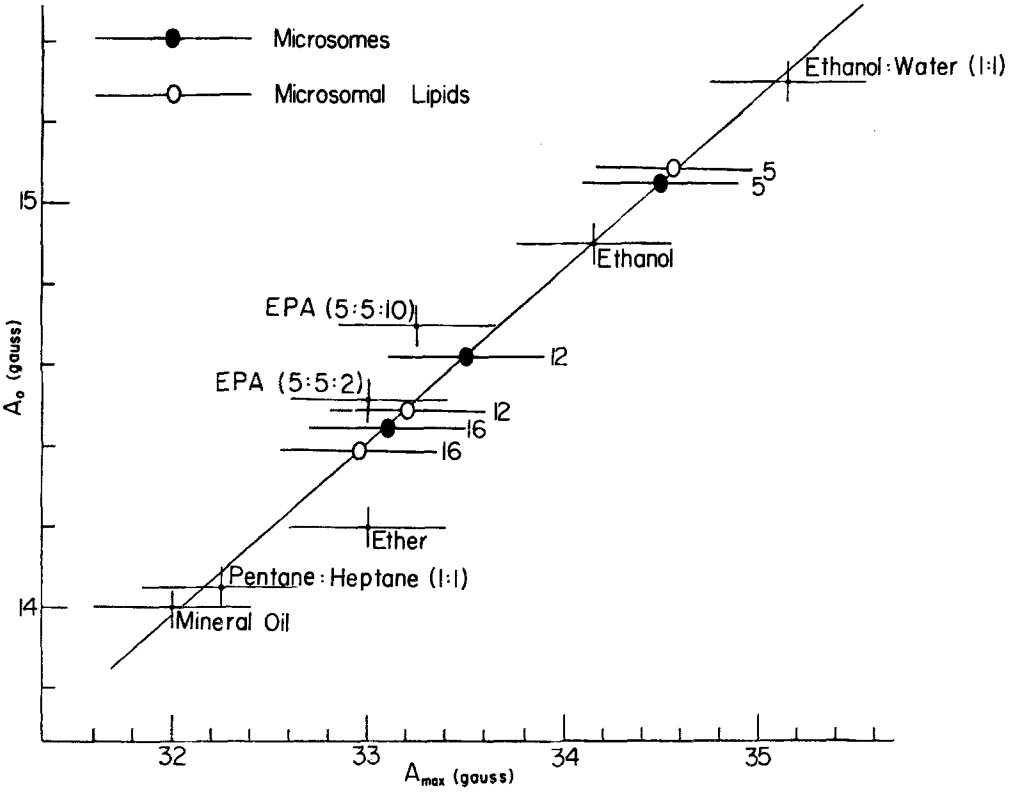

Fig. 4. The solvent dependence of the two nitrogen hyperfine parameters, A_0 and A_{max}. Hyperfine splittings were measured for 5-, 12- and 16-doxylstearic acids in ethanol/water (1:1) and ethanol. To improve the solubility in hydrocarbon solvents at low temperature, the methyl esters of 5-, 12- and 16-doxylstearic acids were used to obtain A_0 and A_{max} values in diethyl ether/2-methyl butane (1:1), and mineral oil. In ethanol, the fatty acid spin labels and the methyl esters yield the same A_0 and A_{max} values within experimental error. No other solvents were examined using both the fatty acids and methyl esters. A_{max} values for the solvents, microsomal lipid vesicles and membranes of the microsomal fraction were determined at -196 °C

the local spin label concentration to the point where electron-electron dipolar and exchange interactions become significant.

The points for the microsomal lipids and membranes of the microsomal fraction are discussed below. Since the corresponding A_0 values were not readily measurable from the spectra, the A_{max} values are plotted on the standard curve of Fig. 4. We note from this combined figure that there is a polarity gradient, and it is very nearly the same in the membrane fraction and the isolated lipids. The label at the C_5 position is experiencing an environment more polar than ethanol, whereas labels at the C_{12} and C_{16} positions are in a somewhat more hydrocarbon-like environment. This

effect must be caused by the bilayer structure since the same spin labels in homogeneous solvents of Fig. 4 do not exhibit this marked dependence of A_{max} with position along the lipid chain.

Lipid Spin Labels in Phospholipid Vesicles and Membranes

Representative room-temperature ESR spectra of the 5-, 12- and 16-doxylstearic acid spin labels diffused into microsomal lipid vesicles and membranes of the microsomal fraction are shown in Fig. 5. The spectral lines become narrower and the splittings decrease as the doxyl group is moved along the fatty acid chain from the C_5 to the C_{12} and finally to the C_{16} position. The same effect was observed when the spin-labeled phospholipids V and VI were diffused into microsomal lipid vesicles (not shown).

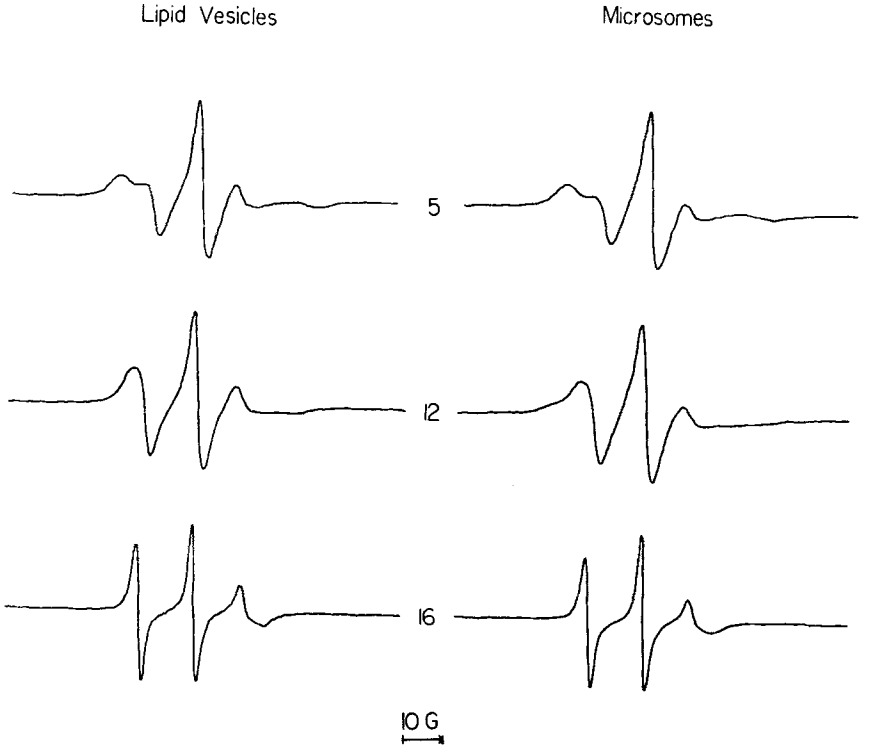

Fig. 5. 9.5 GHz ESR spectra, from top to bottom, respectively, of 5-, 12- and 16-doxylstearic acids in microsomal lipid vesicles (1:200) and membranes of the microsomal fraction (1:200). The numbers in parentheses are the weight ratios of the spin label to lipid in the vesicle samples, or to the protein of the membrane fraction, respectively.The samples were suspended in 0.1 M potassium phosphate buffer, pH 6.5. ESR spectra were recorded at room temperature and the digitalized data have been replotted to the same vertical scale

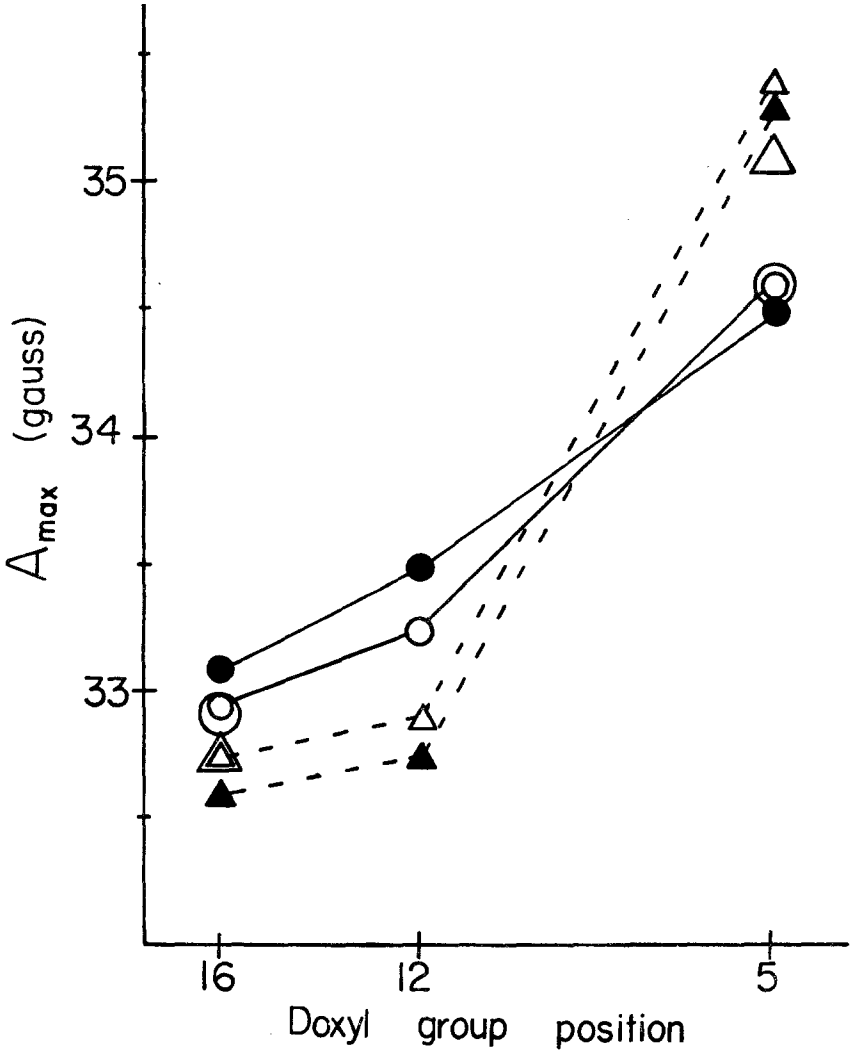

Fig. 6. Variation of the ESR parameter A_{max} with doxyl group position along the hydrocarbon chains. There are two systems, one relating to the microsomal fraction (circles) and the other derived from myelin (triangles). Within these two groups the six sets of data are for doxylstearic acid spin labels II–IV in microsomal lipid vesicles (○), phospholipid spin labels V, VI in microsomal lipid vesicles (◯), II–IV in membranes of the microsomal fraction (●), II–IV in myelin lipid vesicles (△), V and VI in myelin lipid vesicles (△) and II–IV in myelin (▲). All samples were suspended by sonication in 0.1 M potassium phosphate buffer, pH 6.5. The weight ratio of spin label to lipid in the two lipid samples was 1:200 for II–IV and 1:100 for V, VI. The ratio of II–IV to protein (w/w) in the two membrane preparations was 1:200

This is a direct result of the increased molecular motion (i.e. fluidity gradient) along the fatty acid chains, culminating in marked fluidity near the center of the bilayers. Furthermore, the spectra in the right column of Fig. 5 are

very nearly identical to the corresponding spectra in the left column. This provides strong evidence that the membranes of the microsomal fraction contain fluid bilayer regions and that the lipid spin labels are intercalated into these regions. These kinds of observations are not new. Fig. 5 serves primarily as a control to show that the spin-labeled lipid vesicles and membranes of the microsomal fraction exhibit the behavior observed previously in lecithin and lecithin-cholesterol mixtures (Waggoner *et al.*, 1969; Hubbell & McConnell, 1971; Jost *et al.*, 1971*a*; McConnell & McFarland, 1972), several biological membranes (Rottem, Hubbell, Hayflick & McConnell, 1970; Hubbell & McConnell, 1971) and the fluid components of membranous cytochrome oxidase (Jost, Griffith, Capaldi & Vanderkooi, 1973).

The principal membrane chosen for this study is from the calf liver microsomal fraction and representative data are shown in Fig. 6. Specific experiments include fatty acid spin labels diffused into microsomal lipid vesicles (Fig. 6, small open circles) and into membranes of the microsomal fraction (small solid circles). Parallel measurements were made in the phospholipid spin labels V and VI in microsomal lipid vesicles (large open circles). The same trends in $A_{\max}$ are observed using either the fatty acid or the phospholipid spin labels (*see* Fig. 6). A similar set of experiments was performed on beef brain myelin and myelin lipids and these data are also plotted in Fig. 6. It should be emphasized that obtaining accurate measurements of the $A_{\max}$ parameter is difficult because of the broad lines and very small shifts. Interpreting these small shifts as due to solvent effects assumes that $A_{\max} \simeq A_{zz}$ (or a constant times A_{zz}) where A_{zz} is the largest of the three principal values of the electron-nuclear hyperfine matrix (Libertini & Griffith, 1970). $A_{\max}$ equals A_{zz} only in the absence of molecular motion and nitroxide-nitroxide interactions. There is probably some residual molecular motion at -196 °C (e.g. torsional oscillations, methyl group rotations) but these effects contribute to all measurements and do not greatly affect the conclusions which are based on *relative* values. Other potential sources of error include nonrandomness in the microscopic sample orientation and possible disruption of the samples by ice crystal formation. All $A_{\max}$ values reported in this paper are reproducible to within ± 0.4 G.

The Effects of Dehydration

To examine the effects of hydration and dehydration, microsomal lipid samples were prepared as randomly oriented films on glass wool and equilibrated at 100% relative humidity or dehydrated over phosphorus pentoxide. ESR spectra were recorded at room temperature to check the

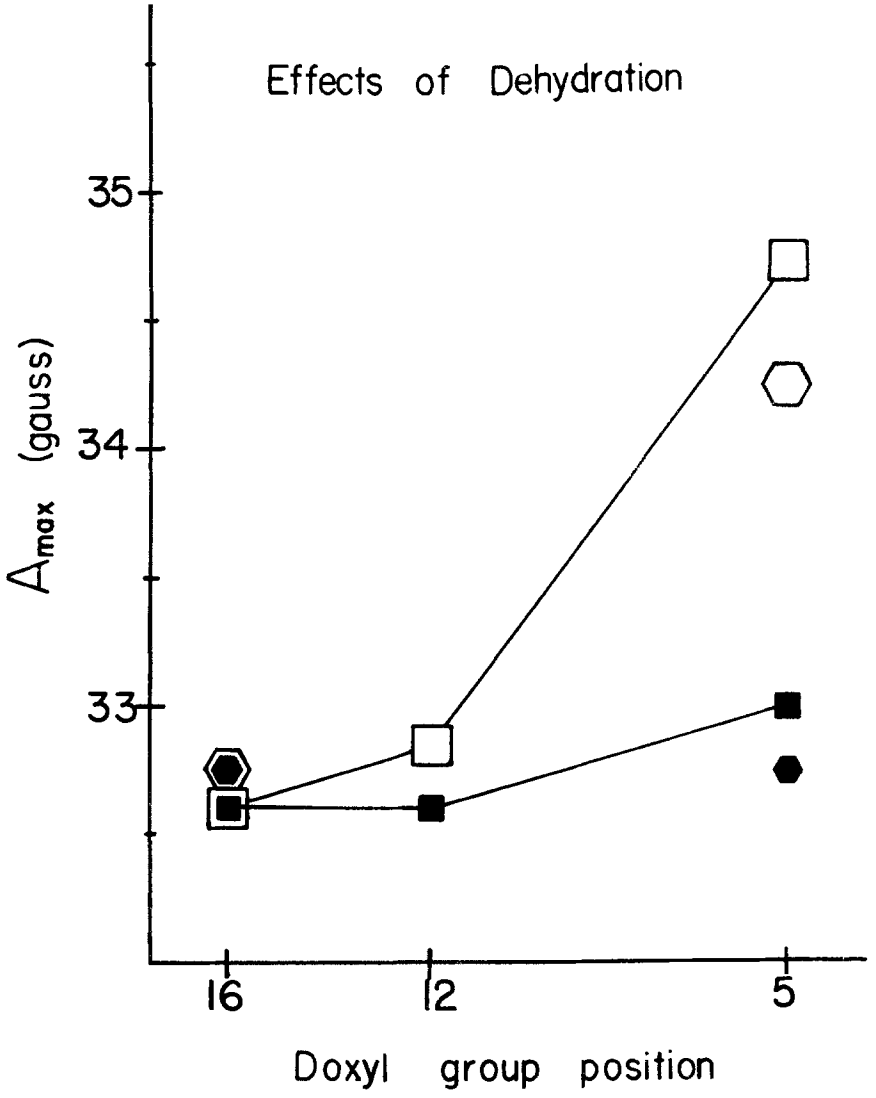

Fig. 7. Effect of dehydration on microsomal lipid vesicles as a function of the doxyl group position along the hydrocarbon chains. The open points (□, ⬡) were recorded for samples that had been equilibrated at 100% relative humidity at room temperature, and the solid points (■, ⬢) were recorded on dehydrated samples. Squares and hexagons represent data obtained using the fatty acid spin labels (II–IV), and the L-α-lecithin spin labels (V, VI), respectively. All samples were frozen at −196 °C before recording the ESR spectra. Lines connect the data points for the fatty acid spin labels. Note the marked effect of dehydration at the C_5 position observed using either the fatty acid or the lecithin spin label

general line shapes (not shown), and then the samples were cooled to −196 °C to obtain the A_{max} values. At room temperature, dehydrating the samples greatly reduces molecular motion at the C_5 position, causes some

reduction of motion at the C_{12} position and has little or no effect at the C_{16} position. These qualitative observations are consistent with the quantitative treatment of motion and orientation effects in spin-labeled egg lecithin samples at room temperature as a function of the relative humidity (Jost *et al.*, 1971*a*).

The A_{max} values obtained from the ESR spectra of the frozen samples are plotted in Fig. 7. The hydrated samples are represented by open symbols. The squares and hexagons represent data obtained with the fatty acid and the phospholipid spin labels, respectively. Both types of spin labels show the marked effect of hydration when the doxyl group is at the C_5 position, near the polar head group region. At the C_{12} position there may be a small effect on A_{max}, although the two points in Fig. 7 lie within the estimated uncertainty of ± 0.4 G. At the C_{16} position, near the center of the bilayers, dehydration produces no observable effect in the A_{max} parameter.

These samples hydrated at 100% relative humidity have, of course, greatly reduced total water content compared to the *aqueous* dispersions of lipid vesicles. Nevertheless, the A_{max} values of the two preparations are very similar, as seen in Figs. 6 and 7. We interpret this agreement as evidence that errors in A_{max} data resulting from any disruption of lipid bilayer structure by ice crystal formation are minimal.

35 GHz ESR Measurements on Di-t-butyl Nitroxide in Aqueous Suspensions of Membranes and Lipid Vesicles

We have also examined the interior of the lipid bilayers by a technique which makes use of the dependence of A_0 and g_0 on solvent polarity. The experiments were patterned after an earlier 35 GHz study on the polarity of lipid vesicles and myelin membrane (Griffith *et al.*, 1971; *see also* Hubbell & McConnell, 1968) and are based on the fact that a small, nearly spherical nitroxide such as di-*t*-butyl nitroxide (I) will exhibit a sharp three-line spectrum in the fluid environment of a phospholipid bilayer. In a concentrated aqueous dispersion of lipid vesicles, the partitioning of I is such that a composite of two ESR spectra is observed, corresponding to I in the lipid environment and in the aqueous phase. The ESR spectrum of I in a lipid environment exhibits a smaller isotropic splitting constant and a slightly increased g value relative to I in an aqueos environment. The net effect is to shift the spectrum of I in lipid downfield and to decrease the peak-to-peak splitting relative to I in the aqueous environment. At 9.5 GHz this results in a superposition of two three-line spectra in which only the high field lines are resolved. However, at 35 GHz both high field and center

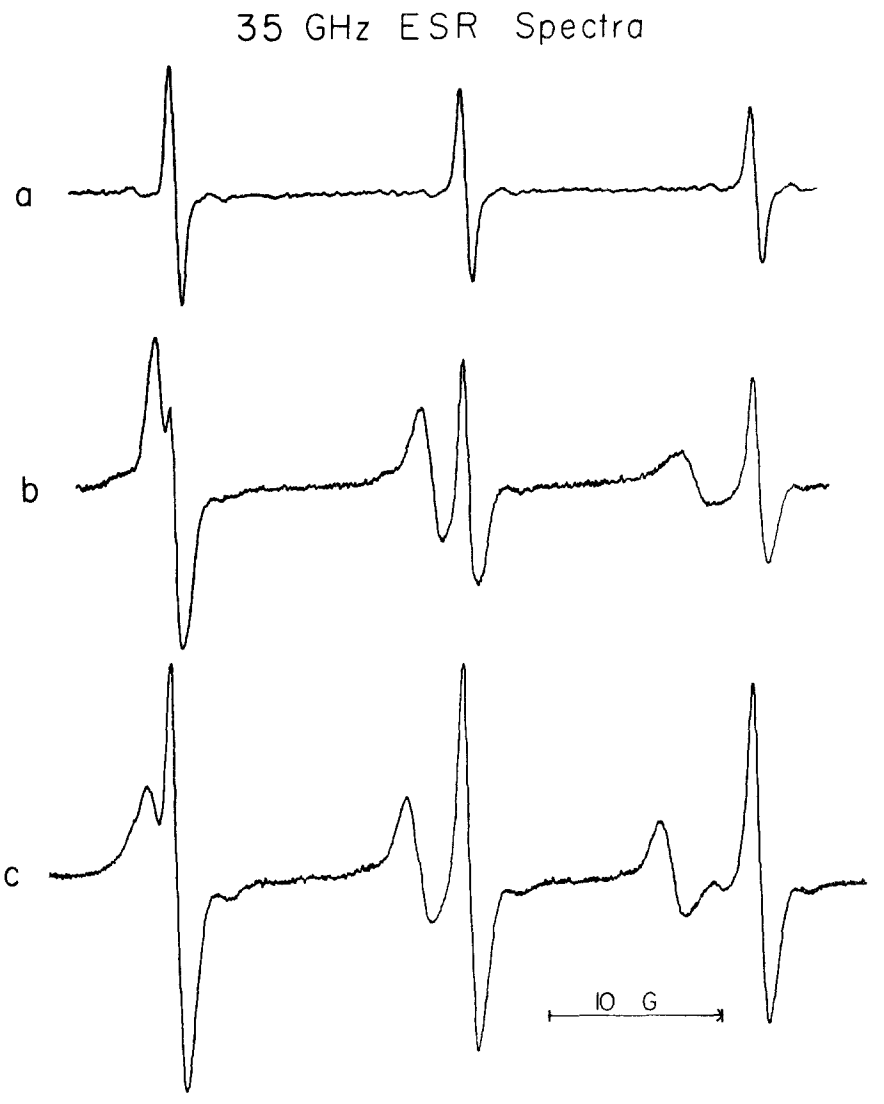

Fig. 8. 35 GHz ESR spectra of di-*t*-butyl nitroxide in (*a*) 0.1 M potassium phosphate buffer, pH 6.5, (*b*) aqueous suspension of membranes of the microsomal fraction, (*c*) aqueous suspension of myelin. All spectra were recorded at room temperature, but not necessarily with the same spectrometer gain

field lines are resolved (and in favorable cases the low field lines are also resolved) (Griffith *et al.*, 1971). Thus, the A_0 and g_0 of I in the lipid environment can be measured using I in aqueous buffer as the standard. ESR spectra recorded at 35 GHz for I in samples of (a) aqueous buffer, (b) aqueous suspension of membranes of the microsomal fraction and (c) aqueous suspension of myelin at room temperature are shown in Fig. 8. From these

Table 2. Isotropic ESR parameters for di-*t*-butyl nitroxide in lipid and membrane samples

Sample	A_0	g_0
Microsomes	15.59	2.0059
Microsomal lipids (vesicles)	15.63	2.0059
Myelin	15.00	2.0061
Myelin lipids (vesicles)	14.93	2.0061

Values were determined from 35 GHz ESR spectra using di-*t*-butyl nitroxide partitioned into the aqueous phase as an internal reference ($A_0 = 17.16$ G and $g_0 = 2.0056$). Estimated uncertainties are ± 0.04 G and ± 0.0002 for A_0 and g_0, respectively, relative to this reference.

spectra both the A_0 and g_0 values of I dissolved in the membranes were readily determined and are listed in Table 2, along with data on the corresponding lipid vesicles.

These data on di-*t*-butyl nitroxide cannot be used to determine the shape of the hydrophobic barrier because the position, or range of positions, of the rapidly tumbling spin label within the bilayer is unknown. However, in contrast to the A_{max} values measured on frozen samples, these 35 GHz data were obtained from samples under very nearly physiological conditions. Thus, the 35 GHz data serve as an important check on the profile determined using the doxyl lipid spin labels, as discussed below.

Discussion

Electronic Structure of Nitroxide-Free Radicals

The solvent dependence of ESR spectra can be most easily visualized as arising from changes in the relative contributions of the two canonical structures of the neutral nitroxide-free radical

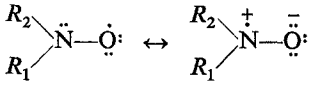

(A) (B)

Structure A localizes the unpaired electron on the oxygen atom whereas structure B localizes the unpaired electron on the nitrogen atom, and is primarily responsible for the three-line ^{14}N hyperfine splitting (the nuclear spin of ^{16}O is zero). Solvents that tend to stabilize the ionic structure (B) will increase the unpaired spin density on nitrogen and, therefore, A_0 and A_{zz}. In adopting this simplified description we neglect several other effects. For example, the formation of charge transfer complexes could reduce the spin

density on *both* the nitrogen and oxygen atoms, rather than to redistribute spin density as implied in structures A and B. Furthermore, there is evidence that the N—O group and the two adjacent tertiary carbon atoms of some nitroxides are not coplanar (Lajzerowicz-Bonneteau, 1968; Berliner, 1970; Capiomont, 1972), and solvent-dependent changes in radical geometry could alter the *s*-orbital contribution and hence the ^{14}N coupling constant.

The Hückel molecular orbital (MO) method and the π-electron approximation provide a useful semiquantitative description. Two π-molecular orbitals are constructed from linear combinations of the $2p_x$ atomic orbitals of nitrogen (χ_N) and oxygen (χ_O). Of the seven electrons of nitrogen in structure A, two are in the nitrogen $1s$ atomic orbital (AO), three are associated with the hybridized σ MO's of the R_1—N, R_2—N and N—O bonds, and the remaining two electrons are in the $2p_z\pi$ orbital. Similarly, the eight electrons of oxygen are distributed as follows: two in the $1s$ AO, one in the $2p_x\sigma$ MO of the N—O bond, a lone pair in the $2s$ AO, a lone pair in the $2p_y$ AO, and one electron in the $2p_z\pi$ orbital. Thus, nitrogen contributes two electrons and oxygen contributes one electron to the two-center π-system.

In the Hückel approximation, the single configuration wave function is

$$\psi=(6)^{-\frac{1}{2}}\sum_p(-1)^p\hat{P}\phi_1\alpha\phi_1\beta\phi_2\alpha \qquad \begin{matrix}\phi_2\uparrow\\ \phi_1\uparrow\downarrow\end{matrix} \tag{1}$$

where

$$\phi_i=C_{i_1}\chi_N+C_{i_2}\chi_O \tag{2}$$

and $\hat{P}$ is the π-electron permutation operator. It is convenient to relate all of the matrix elements of the 2×2 secular determinant to oxygen (rather than carbon, as would normally be the case). Therefore,

$$\langle\chi_O|\hat{\mathscr{H}}|\chi_O\rangle\equiv\alpha_O \tag{3}$$

$$\langle\chi_N|\hat{\mathscr{H}}|\chi_N\rangle\equiv\alpha_N\simeq\alpha_O+h\beta_O \tag{4}$$

$$\langle\chi_N|\hat{\mathscr{H}}|\chi_O\rangle\equiv\beta_{NO}\simeq k\beta_O \tag{5}$$

where $\hat{\mathscr{H}}$ is the one-electron Hamiltonian, α and β are the coulomb and resonance integrals, and h and k are parameters. The energies ($\mathscr{E}_{1,2}$) and the C_{ij}'s are readily determined from the symmetrical 2×2 matrix. The results are

$$\mathscr{E}_{1,2}=\alpha_O+(\tfrac{1}{2})\{h\pm(h^2+4k^2)^{\frac{1}{2}}\}\beta_O \tag{6}$$

$$\phi_2 = -\sin\theta\chi_N + \cos\theta\chi_O \tag{7}$$

$$\phi_1 = \cos\theta\chi_N + \sin\theta\chi_O \tag{8}$$

where

$$\sin^2\theta = (\tfrac{1}{2})\{1 - h(h^2+4k^2)^{-\frac{1}{2}}\} \tag{9}$$

and $\mathscr{E}_1$ is associated with the plus sign in Eq. (6). In the Hückel approximation, the spin density on nitrogen (ρ_N) is the square of the AO coefficient of the MO occupied by the unpaired electron; hence $\rho_N = \sin^2\theta$. The isotropic coupling constant (A_0) is related to ρ_N through the Karplus-Fraenkel relation (Karplus & Fraenkel, 1961; Wertz & Bolton, 1972)

$$A_0 = Q_N\rho_N + Q_{NO}\rho_O \tag{10}$$

where ρ_0 is the π-electron spin density on oxygen and Q_N and Q_{NO} are constants. Evidently $Q_N \simeq 18$ to 24 G and $Q_N \gg Q_{NO}$ (Lemaire & Rassat, 1964; Ayscough & Sargent, 1966; Vasserman & Buchachenko, 1966; Wertz & Bolton, 1972; Cohen & Hoffman, 1973) and for the purposes of discussion, we neglect the small dependence on ρ_0 and simply note that the coupling constants (A_0, A_{zz}, etc.) vary linearly with ρ_N so that, for example,

$$\Delta A_0 = Q_N \Delta\rho_N \tag{11}$$

where $\Delta\rho_N$ and ΔA_0 are the changes in ρ_N and A_0 caused by solvent perturbations or external electric fields. The choices of parameters h and k are not critical since we are concerned with $\Delta\rho_N$, and not the absolute value of ρ_N. A reasonable but somewhat arbitrary choice of parameters is $k = 1$ and $h = X_N - X_O = 3.0 - 3.5 = -0.5$, where X_N and X_O are Pauling's electronegativities for nitrogen and oxygen (Pauling, 1960; Streitwieser, 1961). With this choice of parameters, $\rho_N = 0.62$ and $\rho_O = (1 - \rho_N) = 0.38$.[1] Literature estimates of ρ_N range from 0.9 to 0.3 and general agreement has not yet been reached on the exact experimental value of ρ_N (Rozantsev & Sholle, 1971).

---

1 The use of the electronegativity scale can best be justified when each atom contributes one electron to the π-system. Since the nitrogen atom contributes two electrons, h may have a smaller negative value (or even a small positive value). The ρ_N calculated for $k=1$ and h values of -1.0, -0.5, 0, $+0.1$ are 0.72, 0.62, 0.50, 0.48, respectively. Because this is a two-center problem, it is the ratio of h/k, rather than the individual values, that determines ρ_N. This MO treatment of the nitroxide-free radical is formally the same as the method used previously for the ether radical RĊHOR (Griffith, 1965).

Solvent Effects on the ^{14}N Splitting Parameters

Taking into account the various intermolecular fields acting on the nitroxide-free radical in a precise way is a formidable task well beyond the scope of this work. However, it is instructive to consider the simple case whereby all perturbations contribute to an average electric field ($\boldsymbol{E}$) in the vicinity of the spin label. The Hamiltonian becomes

$$\hat{\mathscr{H}} = \hat{\mathscr{H}}_0(\boldsymbol{r}_i, \boldsymbol{R}_j) + \hat{\mathscr{H}}'(\boldsymbol{E}, \boldsymbol{r}_i, \boldsymbol{R}_j) \tag{12}$$

where $\hat{\mathscr{H}}_0(\boldsymbol{r}_i, \boldsymbol{R}_j)$ is the Hamiltonian in the absence of the electric field, and $\boldsymbol{r}_i$ and $\boldsymbol{R}_j$ denote the vectors from the origin to the positions of the i^{th} electron and j^{th} nucleus, respectively. $\hat{\mathscr{H}}'(\boldsymbol{E}, \boldsymbol{r}_i, \boldsymbol{R}_j)$ represents the electric field perturbation. In the simple molecular orbital treatment the nuclei are fixed and the perturbation takes the form

$$\hat{\mathscr{H}}'(\boldsymbol{E}, \boldsymbol{r}_i) = -e\boldsymbol{E} \cdot \boldsymbol{r}_i. \tag{13}$$

First order perturbation theory using Eq. (13) and the unperturbed energies and eigenfunctions [Eqs. (6)–(8)] leads to the general equation

$$\Delta\rho_{\mathrm{N}} = C_1 E_x + C_2 E_x^2 \tag{14}$$

and the spin density increases with the component of the electric field along the N—O bond (the x-axis). Terms linear and quadratic in E are present, but the linear term is dominant.

Neglecting terms of the type $\langle \chi_{\mathrm{N}} \chi_{\mathrm{O}} e\boldsymbol{r} \rangle$, which is consistent with the Milliken approximation combined with the neglect of differential overlap in the HMO method (Daudel, Lefebvre & Moser, 1959), the coefficient of the linear term reduces to

$$C_1 = 2e\beta^{-1} k^2 (h^2 + 4k^2)^{\frac{3}{2}} r_{\mathrm{NO}} \tag{15}$$

where r_{NO} is the N—O bond length. Assuming $h = -0.5$, $k = 1$, $|\beta| = 2.5$ eV (from Eq. (6) and the $\pi - \pi^*$ optical absorption band at 240 nm), and $r_{\mathrm{NO}} = 1.3$ Å (Berliner, 1970; Boyens & Kruger, 1970) then $C_1 = 1.5 \times 10^{-9}$ (volts/cm)$^{-1}$ so that from Eq. (11) an electric field of 10^7 volt/cm could produce a change in the A_0 component of 0.4 G on an oriented sample. Thus, HMO theory predicts that 10^6 to 10^8 volts/cm corresponds to a measurable effect on the ^{14}N hyperfine splitting. Statistical effects will, of course, alter these figures.

The average electric field is the vector sum, $\boldsymbol{E}=\sum_i \boldsymbol{E}_i$, where the $\boldsymbol{E}_i$'s are associated with nearby molecules and ions. Neglecting quadratic terms, it follows from Eqs. (11) and (14) that $\Delta A_i \propto E_{xi}$, and we may write ΔA (the total change in A) as a sum of terms

$$\Delta A=\Delta A_l+\Delta A_{pd}+\Delta A_{id}+\Delta A_h+\Delta A_s+\Delta A_{dl}+\Delta A_\phi. \tag{16}$$

The first three terms on the right-hand side of Eq. (16) are associated, respectively, with London (dispersion) forces, permanent electric dipole interactions and induced dipole interactions between the nitroxide moiety and the surrounding solvent molecules (the permanent dipole moment of the C—NO—C group is about 3 Debye (Rozantsev, 1970)). As is commonly done, we group these three terms together as van der Waals interactions, and designate the total effect as one term, ΔA_v. The fourth term ΔA_h is the hydrogen bonding term, separated out from ΔA_v because of its special significance. The fifth term ΔA_s represents specific interactions other than hydrogen bonding (e.g. charge-transfer complexes). The next term ΔA_{dl} arises from the charged double layer of phospholipid polar groups. The final term ΔA_ϕ corresponds to the potential that may exist across the membrane.

To assess the relative importance of these various terms in membranes, we consider first the simpler case of homogeneous solutions. Eq. (16) reduces to

$$\Delta A=\Delta A_v+\Delta A_h+\Delta A_s \tag{17}$$

and in solvents that do not form specific (directional) interactions with the N—O group, ΔA_h and ΔA_s also vanish. In this case the solvent can be regarded as a continuous medium of dielectric constant ε and the Onsager model (Onsager, 1936) may be used to relate the local electric field and hence ΔA to the dielectric constant. According to the Onsager model, when the polar molecule (e.g. nitroxide) is dissolved, it polarizes the solvent molecules and this polarization gives rise to an electric field E_R (Onsager's "reaction field"). Representing the nitroxide as a sphere of radius r, with a point electric dipole of moment μ at the center, immersed in the continuous medium of dielectric constant ε, then the magnitude of the electric field experienced by the nitroxide is

$$E_R=\frac{2(\varepsilon-1)(n_D^2+2)}{3(2\varepsilon+n_D^2)}\frac{\mu}{r^3} \tag{18}$$

where n_D is the refractive index of the pure nitroxide (Onsager, 1936). For di-*t*-butyl nitroxide, $\mu \simeq 3$ Debye, $n_D^2 \simeq 2$ and $r \simeq 4$ Å, for a density of 0.86

(Rozantsev, 1970). With these numerical values Eq. (18) reduces to

$$E_R \simeq \frac{(\varepsilon-1)}{(\varepsilon+1)} 1.8 \times 10^7 \text{ V/cm}. \tag{19}$$

The direction of E_R is along the permanent electric dipole moment, and since the N—O bond moment dominates the total dipole moment of di-*t*-butyl nitroxide, this field will be very nearly parallel to the N—O bond (the x-axis).

Eq. (19) is useful in (1) selecting a reference point for the definition of ΔA, (2) determining which solvents contribute ΔA_h or ΔA_s terms, and (3) estimating the magnitude of the electric field required to produce a measurable ΔA_0. For example, defining $\Delta A_0 \equiv A_0 - A_0^{\varepsilon=1}$ and requiring $\Delta A_0 \to 0$ as $(\varepsilon-1)/(\varepsilon+1) \to 0$ we find from the data of Table 1 (excluding water, the alcohols and formamides) and using published dielectric constants (e.g., Handbook of Chemistry and Physics, 1972) that $A_0^{\varepsilon=1}$ of di-*t*-butyl nitroxide is 14.85 ± 0.05 G. Physically, $A_0^{\varepsilon=1}$ corresponds to the spin label in a region where the local electric fields are essentially zero, as in a dilute gas. (Accurate gas phase coupling constants of nitroxide-free radicals are troublesome to obtain because of spin-rotation interaction.) A plot of $\Delta A_0 = A_0 - 14.85$ G *vs.* the function $(\varepsilon-1)/(\varepsilon+1)$ is shown in Fig. 9 for di-*t*-butyl nitroxide in the solvents of Table 1. The points clearly fall into two groups. In most solvents there is a linear dependence of ΔA_0 on the function $(\varepsilon-1)/(\varepsilon+1)$. The notable exceptions are the alcohols and aqueous solutions (Fig. 9, Nos. 19–22, 24–28, 30–33). To a lesser degree the primary or secondary amides are also exceptions (Fig. 9, Nos. 23 and 29). The other solvents of Table 1 do not yield large ΔA_h or ΔA_s terms, as judged by this criterion. Fig. 9 and Eq. (19) together provide a method of relating the electric field and ΔA_0. The slope of the lower curve of Fig. 9 is 0.8, hence from Eq. (19) $\Delta A_0 = 0.8\, E_R/1.8\,(10)^7$ V/cm. Thus an electric field of 10^7 V/cm corresponds to a ΔA_0 of about 0.4 G. This agrees, perhaps somewhat fortuitously, with the estimate obtained independently from the molecular orbital calculation.

Nitroxide-free radicals are Lewis bases. Numerous interesting ESR, IR, optical and NMR contact shift studies of interactions of nitroxides with alcohols, aqueous solutions, amines, amides, halogen-substituted hydrocarbons, unsaturated molecules, chloranil, tetracyanoethylene, $CoBr_2$, $GeCl_4$, $TiBr_4$, $AlCl_3$ and related complex-forming reagents have been reported (Briere, Rassat, Rey & Tchoubar, 1966; Sysoeva, Stepanyants & Buchachenko, 1968; Brown, Maier & Drago, 1971; Lim & Drago, 1971;

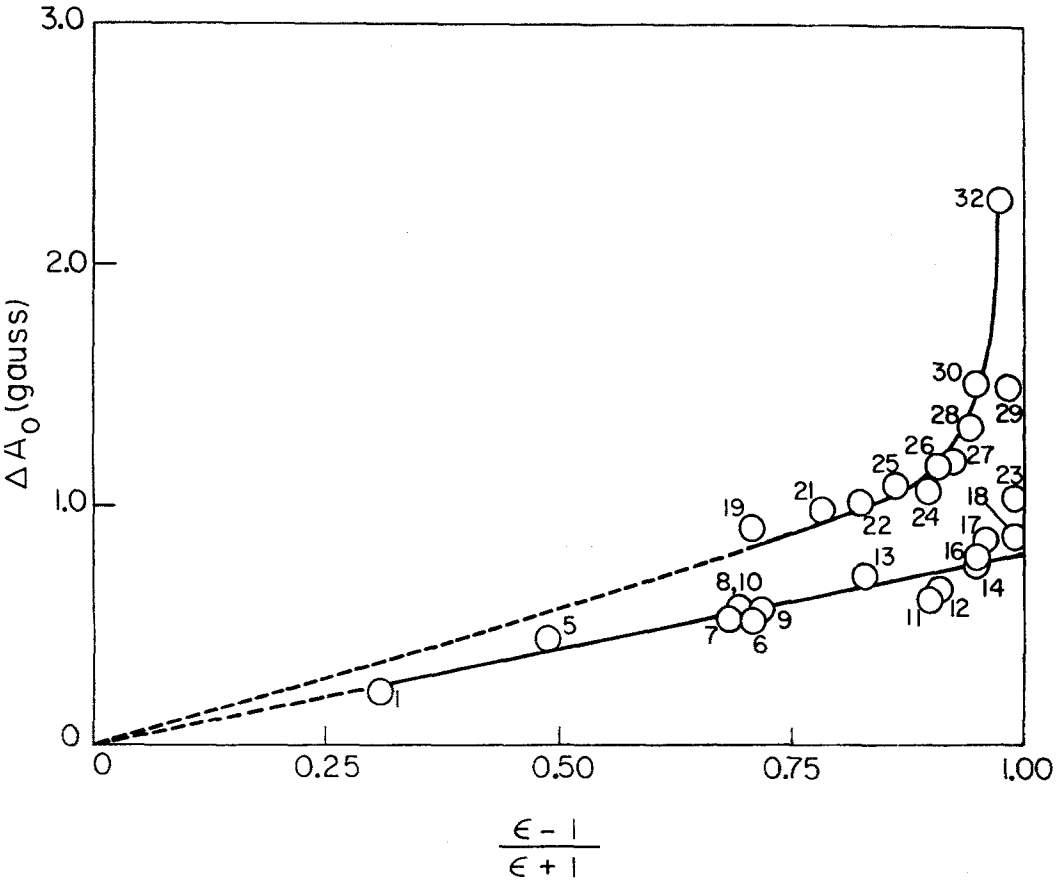

Fig. 9. Plot of $\Delta A_0 = A_0 - A_0^{\varepsilon=1}$ for di-*t*-butyl nitroxide *vs.* the function $(\varepsilon-1)/(\varepsilon+1)$, where ε is the dielectric constant of the solvent at room temperature. The constant $A_0^{\varepsilon=1} = 14.85 \pm 0.05$ G was determined by extrapolation, requiring $\Delta A_0 \to 0$ as $(\varepsilon-1)/(\varepsilon+1) \to 0$. The solvents and A_0 values are from Table 1. A few solvents of Table 1 are omitted from this plot for lack of dielectric constant data

Murata & Mataga, 1971; Cohen & Hoffman, 1973; Kabankin, Zhidomirov & Buchachenko, 1973). Since our aim is to interpret the ΔA values observed in phospholipid bilayers, rather than to examine solvent effects in general, we neglect all but the major effects and consider only those brought about by functional groups likely to be encountered in aqueous phospholipid vesicles. Thus, we neglect all ΔA_s terms but we conclude from Fig. 9 that *hydrogen bonding contributes significant* ΔA_h *terms if spin labels are in contact with water or alcohols.*

A test of the penetration of water molecules into phospholipid bilayers is provided by the dehydration data of Fig. 6. Although dehydration may also cause molecular rearrangements, the magnitude and direction of the

observed change in A_{max} values can only be accounted for by the removal of water molecules from the vicinity of the nitroxide groups. Therefore, we conclude that *in aqueous or hydrated samples, water molecules do penetrate into the phospholipid bilayer regions.* To account for the large effect at the C_5 position the oxygen of the water molecules must penetrate to at least the C_2 position (i.e. adjacent to the carboxyl group, on the hydrocarbon side), in order to establish the normal O—H···O hydrogen bonding distance of 2.8 Å (Pauling, 1960). The small response at the C_{12} position could reflect infrequent water penetration up to one-fourth the width of the bilayer, but the size of the response is approaching the experimental error so that this cannot be claimed with certainty. There is no effect of dehydration within experimental error at the C_{16} position (*see* Fig. 6).

A potential difficulty in all spin labeling experiments is the perturbation introduced by the label itself. In this study we must ask (1) whether the lipid with the doxyl group covalently attached is in register with the other lipids and not perhaps extending slightly further into the aqueous interface, and (2) whether the water molecules detected by the spin label actually penetrate in the absence of the spin label. These questions cannot be fully answered. The purpose in using both the fatty acid spin labels II–IV and the phospholipid spin labels V, VI was to test the first point. The fact that the same polarity effects and dehydration effects were obtained with either type of spin label argues for the validity of these measurements. Regarding the second point, if the water molecules were adjacent to the doxyl group at the C_5 position solely because of the tendency of the N—O moiety to form hydrogen bonds, then hydration of the 12-doxyl and 16-doxyl lipids would also be expected and this is not observed. Finally, we note that the large and reversible changes in molecular motion and orientation observed at room temperature with changes in relative humidity argue for hydration of the bulk phase surrounding the spin-labeled lipids (Jost *et al.*, 1971*a*).

Charged Double Layer and the Membrane Potential

The remaining two terms, ΔA_{dl} and ΔA_{ϕ}, of Eq. (16) are present only in the bilayers or membranes. The effects of the charged double layer can be approximated by high ionic strength aqueous salt solutions for sites *within* the double layer. On the other hand, when the spin labels are in the *interior* of the bilayer the long range effects of the charged double layer are not readily evaluated using data on homogeneous solvents. We approach this problem by calculating the electric field caused by the charged double layer as a function of the distance into the hydrophobic interior of the bilayer. If each double layer could be represented by a pair of infinite plane

sheets with *uniform* charge per unit area of $+\sigma$ and $-\sigma$, separated by a distance a, then the electric potential ϕ at points beyond the pair of infinite plane sheets is constant and the electric field is zero. However, the molecular dimensions are important. The repeat distance (b) between phosphate groups is not negligible compared to the distance (s) measured from the phosphate group to a site (Y) along the hydrocarbon chain (perpendicular to the double layer), and the assumption of *continuous* plane sheets of charge is questionable. We consider instead a two-dimensional grid of charged pairs representing the negatively charged phosphate groups and the positively charged amines of each phospholipid molecule on one side of the membrane. A second two-dimensional grid of opposite polarity is then placed a distance d away to represent the double layer on the opposite side of the membrane. The conformations of the polar groups are uncertain and probably change with the state of hydration. For the purpose of estimating the magnitude of ΔA_{dl} we take the two hexagonal arrays of charged groups shown in Fig. 10. In one extreme the polar groups are extended normal to the bilayer plane. The phosphate groups and protonated amines are denoted by negative and positive point charges, respectively. The positive charges in the view normal to the bilayer plane are not shown in Fig. 10. They are located directly behind the negative charges when viewed from point Y. In the other extreme case the polar head groups are bent 90°. The double layer is collapsed, moving the positive charges to the positions marked with circles in Fig. 10 (i.e. the charges are coplanar). The electrostatic potential (ϕ) at point Y caused by one double layer of either type is simply the sum of potentials (ϕ_{ij}) due to the charged pairs, so that $\phi = \Sigma\phi_{ij}$ where $\phi_{ij} = q(4\pi\varepsilon)^{-1}(1/r_1^{ij} - 1/r_2^{ij})$ and r_1 and r_2 are the distances from Y to the negative and positive centers, respectively, of the ij^{th} charged pair. The effects of the second double layer are treated similarly. With $a = 5$ Å, $b = 10$ Å, $d = 52$ Å, a grid size of 10^4 charged pairs, and assuming an average dielectric constant of $\varepsilon = 2$ within the bilayer, the electric field perpendicular to the bilayer plane in the extended double layer model is approximately (in V/cm): 1×10^7, 2×10^5, 7×10^3 and $< 10^3$ when s is 5, 10, 15 and 20 Å, respectively. In the collapsed double layer model the corresponding values of the electric field at these distances are 1×10^7, 3×10^5, 9×10^3 and $< 10^3$ V/cm, respectively. The N—O groups of the 5-, 12- and 16-doxyl lipids in the all trans configuration are estimated to be at $s \simeq 9$, 18 and 21 Å, respectively. The electric field at 9 Å is 5×10^5 V/cm in the extended double layer model and 7×10^5 V/cm in the collapsed double layer limit. In both models the electric field is less than 5×10^{-3} V/cm at 18 and 21 Å. Thus, the magnitudes of the electric field calculated from these two models are quite similar.

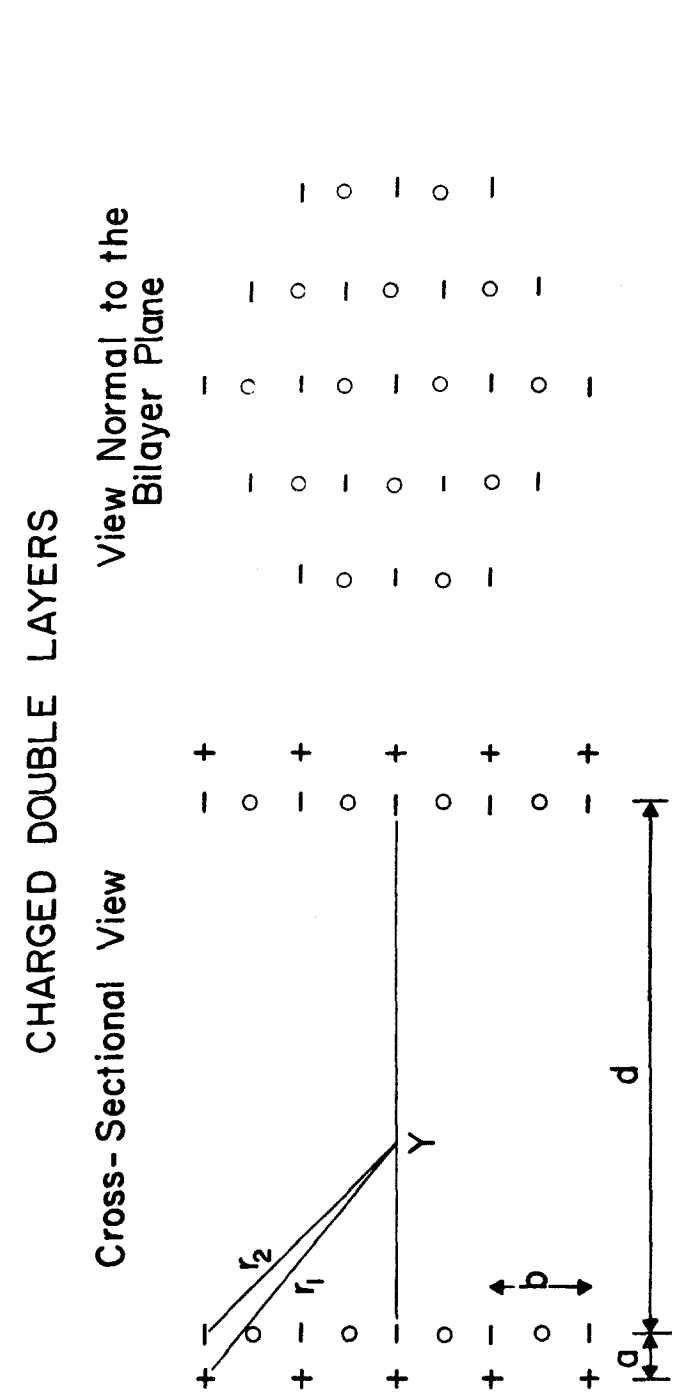

Fig. 10. The configuration of charges upon which the electric fields of the double layer are calculated. Negative signs represent phosphate groups and positive signs indicate the protonated amines in the fully extended configuration. The circles are positions of the protonated amines in the collapsed double layer limit. These two extremes of fully extended and collapsed double layer provide the basis for estimating the range of effects on lipid spin labels intercalated into the phospholipid bilayers

To estimate the *upper limit* to ΔA_{dl} we assume that the electric field is parallel to the N—O bonds. Experimentally, it is known that a Gaussian distribution of orientations exists in which the N—O bonds attached to the fatty acid chains are more nearly perpendicular to the normal, greatly reducing the effect of the electrical field (Libertini, Waggoner, Jost & Griffith, 1969). The alignment is greatest near the polar head groups and becomes progressively more random towards the center of the bilayer. This means that where the electric field is the strongest, the orientation of the N—O group minimizes ΔA_{dl}. Farther down the hydrocarbon chain a fraction of the N—O groups occupy more favorable orientations but at these distances from the double layer the electric field has become very weak. From Eqs. (11), (14) and (15), an electric field of 7×10^5 V/cm (parallel to the N—O bond) corresponds to $\Delta A_{dl} \simeq 0.02$ G. Although this is only an order of magnitude estimate, the effect at the C_5 position is predicted to be very small. The influence of the double layer decreases rapidly with distance and is essentially zero at the C_{12} and C_{16} positions (and identically zero by symmetry at the center of the bilayer). Only at positions very near the double layer does ΔA_{dl} become significant. For example, if the doxyl moiety were 5 Å from the phosphate group (e.g. a hypothetical 2-doxyl derivative) then the electric field is calculated to be 1×10^7 V/cm, yielding $\Delta A_{dl} \simeq 0.4$ G. (Again, this is an upper limit.)

The double layers of Fig. 10 correspond to electrically neutral phospholipid vesicles. Introducing a net charge is readily accomplished by moving an occasional charge a short distance away from the grid. For example, with a few positive charges displaced along a normal to the bilayer plane, the surface carries a net negative charge and the displaced positive charges now represent counter ions of the diffuse Gouy-Chapman layer. The system composed of the counter ions and vesicles remains electrically neutral. It is convenient to neglect the diffuse nature of the double layer and assume all neutralizing counter ions exist in a single plane, a distance a' from the array of negative charges (i.e. the Helmholtz approximation) (Mysels, 1959). With this approximation we need only modify Fig. 10 by displacing a few charges before calculating the electric potential (or, equivalently, adding the potential of a displaced coarse grid of opposite polarity to the potential already obtained for the grids of Fig. 10). Calculations were performed on the extended double layer model with $a' = 2a$, $5a$ and $10a$, and displacements at sites $b' = n\,2b$, $n\,3b$, $n\,10b$ or $n\,100b$ where $n = 0, 1, 2 \ldots$ (i.e., a negative charge and counter ion in line with Y, and hexagons of negative charges and counter ions at $2b$, $4b$, $6b \ldots$ or as few as $100b$, $200b \ldots$ etc.). The results are not of sufficient value to present in detail here. There is an

increase in the electric field because the displaced positive charges are surrounded by water ($\varepsilon \simeq 80$) and these charges are effectively screened, leaving behind the effect of the negative charges. However, we find that the corresponding changes in ΔA_{dl} are not large enough to be considered significant at the C_5, C_{12} and C_{16} positions. Water penetration will tend to increase the average dielectric constant between the double layer and the N—O groups, hence increase the screening of all charges, and reduces ΔA_{dl} from the values calculated assuming $\varepsilon = 2$.

The experimental dehydration data of Fig. 7 also suggest that the ΔA_{dl} term is minimal. The primary effect of dehydration is of course to remove the ΔA_h term. Other effects include possible reduction of the charge density, reduction of charge screening and rearrangement of charges of the double layer. The major phospholipids in the microsomal samples are phosphatidylcholine, phosphatidylethanolamine and phosphatidylserine. Any reduction in surface charge density, brought about by reduction in ionization (e.g. carboxyl protons), would be minimal in samples of pure phosphatidylcholine. As a control, the dehydration experiment was repeated with egg phosphatidylcholine and the results are similar to Fig. 7, suggesting that charge reduction does not significantly alter ΔA. Reduction of screening must occur upon dehydration, increasing the effective electric field in the bilayer. But the effect is insignificant, otherwise dehydration would increase ΔA, contrary to the results of Fig. 7. A rearrangement of charges will also occur. However, the above calculations indicate that ΔA_{dl} for two extreme conformations of the polar head groups are similar, so that charge rearrangement is of secondary importance. *We therefore conclude from the points plotted in Fig. 7 that* $\Delta A_{dl} \ll \Delta A_h$ *even at the* C_5 *position. Dehydration effectively abolishes the polarity gradient and renders* A_{max} *almost independent of the doxyl group position in the dry microsomal lipid samples.*[2]

---

2 As this manuscript was nearing completion, we became aware of an interesting recent study of spin-labeled liquid crystals and lipid dispersions by Seelig, Limacher and Bader (1972). These authors indicate that the polarity profile they observe is attributable to electrostatic interactions between the nitroxide and the charged double layer. The experimental systems are different, and it is plausible that the double layers have a larger effect in the liquid crystalline systems they examined (e.g. aqueous mixtures of octanoic acid, decanoic acid, or the corresponding sodium salts and decanol). However, our data on homogeneous solvents, the molecular orbital treatment, the results based on Onsager's model, and electrostatic double layer calculations coupled with the dehydration experiments strongly suggest that the double layer effects are not significant in these *phospholipid bilayers* except when the nitroxide is within a few Angstroms of the charged groups. Water penetration is the dominant effect in the phospholipid vesicles examined here.

The last term, ΔA_ϕ, is not present in the samples examined here, but would be of interest in studies of transport and excitable membranes. As a hypothetical example, we assume that an electrostatic potential of 40 mV is imposed across a membrane of effective thickness of 40 Å. The resulting electric field is 10^5 V/cm, perpendicular to the bilayer plane and the 5-, 12- and 16-doxyl derivatives experience the same electric field. Unfortunately, from Eqs. (11) and (15), this electrostatic field corresponds to $\Delta A_\phi \simeq 4$ mG, which is too small to be observed using present ESR techniques. To optimize the experiment the spin label should be at the center of the bilayer where ΔA_v is minimal and ΔA_{dl} and ΔA_h are essentially zero. In any case, for the purposes of this discussion, ΔA_ϕ is negligible.

Shape of the Hydrophobic Barrier

We now combine the $A_{\max}$ data from spin labels II–IV in microsomal lipids and membranes of the microsomal fraction, the 35 GHz ESR data on I in similar preparations, and the measurements on homogeneous solvents to obtain the approximate shape of the hydrophobic barrier. Several straightforward operations are required to convert all data to a common scale because two different types of spin labels were used (I and II–VI) and two different parameters were measured ($A_{\max}$ and A_0). We select as a common polarity index the isotropic splitting constant of the doxyl fatty acids, A_0(doxyl), and define the quantity $\Delta A_0(\text{doxyl}) \equiv A_0(\text{doxyl}) - A_0^{\varepsilon=1}(\text{doxyl})$ where $A_0^{\varepsilon=1}(\text{doxyl})$ is the isotropic splitting constant in the absence of solvent perturbations. Neglecting minor variations in solvent data of the various positional isomers, the average value of $A_0^{\varepsilon=1} = 13.85 \pm 0.09$ G as determined by extrapolations of homogeneous solvent data similar to the lower curve of Fig. 9. All $A_{\max}$ points are readily converted to the corresponding A_0 values using the standard curve of Fig. 4.

Fig. 11 is a summary of the combined ESR data on microsomal lipid samples. Distances along the horizontal scale were taken from Corey-Pauling-Koltun molecular models and from known dimensions of lipid bilayers and membranes (Thompson & Henn, 1970; Caspar & Kirschner, 1971). Except for the point representing the charged double layer (i.e. 30 Å), all data were obtained with the doxyl spin labels II–VI. The point at 40 Å is simply ΔA_0 for the doxyl fatty acids in water at room temperature. Data points *within* the bilayer are from frozen samples of microsomal lipids and the vertical error bars are large because of difficulties in measuring $A_{\max}$ values accurately from the broad outermost lines of the rigid glass

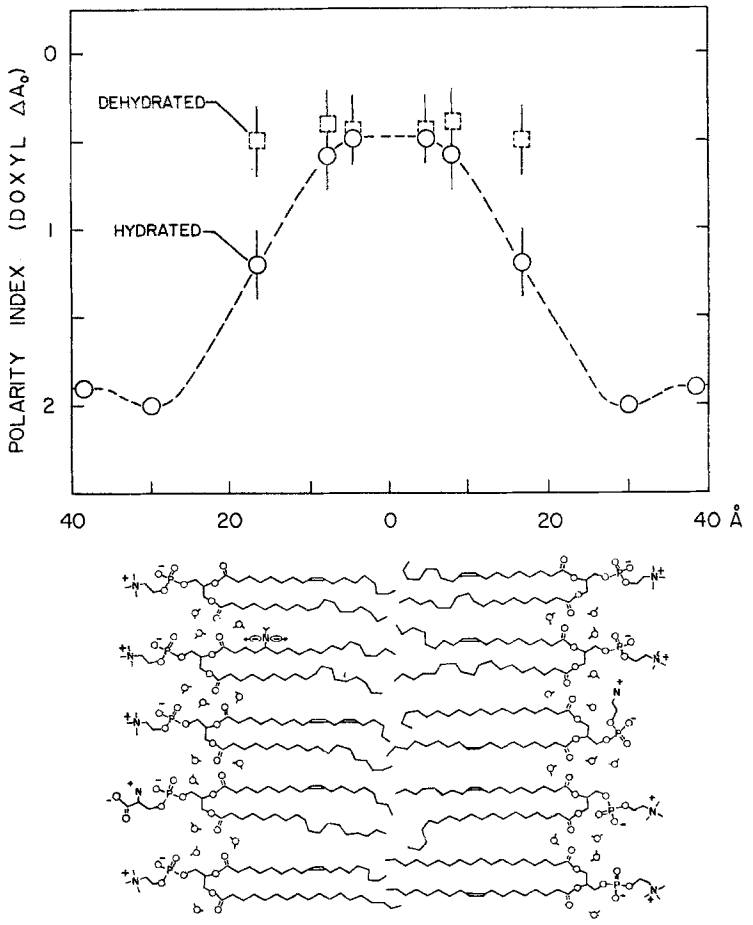

Fig. 11. Shape of the hydrophobic barrier in microsomal lipid bilayers, as derived from spin-labeling data. All data were obtained using spin labels II–VI except the point in the charged double layer region (i.e. 30 Å), which was estimated indirectly from I in concentrated salt solutions (*see text*). The dashed line indicates the shape of the hydrophobic barrier in fully hydrated vesicles of lipids from the microsomal fraction. Below is a cross-sectional sketch of a lipid bilayer including a few water molecules drawn to scale with the normal O—H ··· O hydrogen bonding distance of 2.8 Å

spectra. Microsomal lipid samples containing the fatty acid and the corresponding phospholipid spin labels yielded similar results and these data were averaged before plotting in Fig. 11.

The remaining data are provided by the small spin label, di-*t*-butyl nitroxide (I), in aqueous salt solutions and in microsomal lipid samples at room temperature. The isotropic coupling constant of di-*t*-butyl nitroxide,

A_0(I), is somewhat larger than that of the doxyl lipid spin labels and a conversion factor is required. From homogeneous solvent data we find that the relationship is approximately linear. Specifically, from Table 1 and A_0 values of II and IV measured at 24 °C in the solvents water, water-ethanol (1:1), ethanol, N,N-dimethyl formamide, acetone, ethyl acetate and *n*-hexane, the approximate relationship is $A_0(\text{doxyl}) = 0.80 A_0(\text{I}) + 2.0$. It follows immediately that $\Delta A_0(\text{doxyl}) = 0.80 \Delta A_0(\text{I})$ and this equation is useful in completing Fig. 11. For example, it would be difficult to measure A_0(doxyl) directly in the polar head group region with the spin labels II–VI. If we assume that the double layer can be approximated by a thin layer of aqueous salt solution 3 to 10 Å wide containing, on the average, charged pairs every 8 to 10 Å (as in Fig. 10), then the ionic strength is in the range 2 to 9. For an ionic strength of 5, interpolation between water and 10 M LiCl in Table 1 gives $\Delta A_0(\text{I}) = 2.5$, thus $\Delta A_0(\text{doxyl}) \simeq 0.8 \times 2.5 = 2.0$, which is the number plotted in Fig. 11. Some variation in this estimate would not significantly affect the curve of Fig. 11, but we believe that inclusion of the double layer effects in at least an approximate way is useful. The minima of Fig. 11 suggest a dependence of some transport processes on the ionic strength of the aqueous phases, although this effect could easily be offset by steric and other factors.

In microsomal lipid vesicles at room temperature, $A_0(\text{I}) = 15.63$ G, as measured from the high frequency ESR spectra (Table 2). Therefore, $\Delta A_0(\text{doxyl}) = 0.8 \times (15.63 - 14.85) = 0.62$. This figure is slightly further down on the polarity index than the top portion of the barrier measured with the 12- and 16-doxyl lipids, but the differences are within the combined limits of error. We view this general agreement as evidence that the profile of Fig. 11, obtained largely from frozen samples, is applicable to vesicles and membranes under physiological conditions. A slightly more polar average environment of di-*t*-butyl nitroxide is consistent with the idea that the distribution of this rapidly tumbling small molecule is at a maximum in the central region of the bilayer, and decreases towards the charged double layer, but remains finite in the hydrated regions of the bilayer.

It is tempting at this point to obtain from the spin labeling data a measure of the dielectric constant within the bilayers, and to use this value in the Born equation (Neumcke & Läuger, 1969; Hall, Mead & Szabo, 1973) to estimate the potential energy of ionophores traversing the bilayer. However, we find that neither the present doxyl lipid data nor the di-*t*-butyl nitroxide data are suitable for this calculation. Small changes in coupling constants correspond to large changes in the dielectric constant and the

relationship depends on whether or not hydrogen bonding is present (*see* Fig. 9). The dielectric constant almost certainly varies with position within the bilayer. The most useful value lies near the center of the bilayer and corresponds to the top of the hydrophobic barrier. We note that, in principle, it should be possible to obtain an estimate of this value from the 16-doxyl lipids IV and VI at room temperature using careful line shape analyses, well-oriented samples or zero field spectroscopy.

In an important recent study, Hall, Mead and Szabo (1973) have arrived at an approximate shape of the energy barrier in black lipid (phosphatidylethanolamine) films in the presence of potassium ions and nonactin by fitting current-voltage curves to the Nernst-Planck flux equation, treating the barrier shape as the variable. They conclude that the barrier is trapezoidal. Defining d to be the width of the base and defining n such that $(1-2n)d$ is the width at the top of the trapezoid, these authors find that the best fit of the current-voltage data corresponds roughly to $n \simeq 0.27$ (d is not determined). On this scale, n ranges from zero (rectangular potential) to 0.5 (triangular potential).

The spin-labeling data also suggest a trapezoidal-shaped barrier. The curve of Fig. 11 for the *hydrated* samples is approximated by a trapezoid having $d = 50$ Å and $n \simeq 0.36$. This curve can be refined later with additional positional isomers of the spin labels (C_3 through C_{18}). The experiments are of course different. The current-voltage curves involve positively charged complexes in lipid bilayers whereas the spin-labeling experiments involve the stabilization of polar structures in lipid bilayers. For this reason we prefer a qualitative comparison of curve shapes rather than an emphasis on quantitative curve fitting.

It is interesting to note that water structure plays an important role in determining the shape of the barrier. The points of Fig. 11 from the dehydrated samples correspond to a trapezoid with $n \simeq 0.19$, a shape approaching a rectangular barrier. The calculations based on Fig. 10 suggest it is water penetration and not changes in conformation of the polar head groups with hydration that bring about this change in ESR parameters. We note from Figs. 4 and 6 that the barrier shape is essentially the same in the microsomal lipid vesicles and membranes of the microsomal fraction. This is consistent with the interpretation that the dominant spectral component represents lipid spin labels intercalated into bilayer regions of the membranes. Finally, some data were also obtained on beef brain myelin and myelin lipids. Here again the lipids and membranes yield very similar ESR spectral

parameters. However, there are differences between the microsomal and myelin results as seen in both the frozen samples and in the 35 GHz ESR data (Fig. 6 and Table 2). The data on myelin and myelin lipids also fit a trapezoidal curve and the polarity index of the base is necessarily the same as in Fig. 11. However, the sides of the trapezoid rise more steeply, the top of the trapezoid is higher on the scale, indicating a more hydrocarbon-like environment, and $n \simeq 0.30$. No detailed study of these differences has been attempted. They are presumably caused by a combination of decreased water penetration, and different lipid composition. We mention these results on myelin because the comparison provides a note of caution that the detailed shape of the hydrophobic barrier is not a universal property and does vary with the membrane composition.

It is our pleasure to acknowledge the help and advice we have received from Dr. Charles Burke, Dr. Patricia Jost, Thomas Marriott and Thomas Micka.

Financial support by U.S. Public Health Service Grants CA 10337 and 1 KO4 CA 23359 from the National Cancer Institute is gratefully acknowledged. P.J.D. was aided by Grant No. PF-815 from the American Cancer Society.

References

Ayscough, P. B., Sargent, F. P. 1966. Electron spin resonance studies of radicals and radical-ions in solution. Part V. Solvent effects on the spectra of mono- and di-phenyl nitric oxide. *J. Chem. Soc. (London) B.* **1966**:907

Berliner, L. J. 1970. Refinement and location of hydrogen atoms in nitroxide 2,2,6,6-tetramethyl-4-piperidinol-1-oxyl. *Acta Cryst.* **B26**:1198

Birrell, G. B., Van, S. P., Griffith, O. H. 1973. Electron spin resonance of spin labels in organic inclusion crystals. Models for anisotropic motion in biological membranes. *J. Amer. Chem. Soc.* **95**:2451

Boeyens, J. C. A., Kruger, G. J. 1970. Remeasurements of the structure of potassium 2,2,5,5-tetramethyl-3-carboxypyrroline-1-oxyl. *Acta Cryst.* **B26**:668

Branton, D., Deamer, D. W. 1972. Membrane Structure. Springer-Verlag, New York

Briere, R., Lemaire, H., Rassat, A. 1965. Nitroxydes. XV. Synthese et etude de radicaux libres stables piperidiniques et pyrrolidinique. *Bull. Soc. Chim. France* **32**:3273

Briere, R., Rassat, A., Rey, P., Tchoubar, B. 1966. Nitroxydes. XXI. Mise en evidence par resonance paramagnetique electronique de l'effet specifique des sels sur la solvation des radicaux nitroxydes. *J. Chim. Phys.* **63**:1575

Brown, D. G., Maier, T., Drago, R. S. 1971. Cobalt (II) complexes of the free-radical ligand di-*tert*-butyl nitroxide. *Inorg. Chem.* **10**:2804

Capiomont, A. 1972. Structure cristalline du radical nitroxyde: suberate de di-tetramethyl-2,2,6,6-piperidinyl-4-oxyle 1. *Acta Cryst.* **B28**:2298

Caspar, D. L. D., Kirschner, D. A. 1971. Myelin membrane structure at 10 Å resolution. *Nature, New Biol.* **231**:46

Cohen, A. H., Hoffman, B. M. 1973. Hyperfine interactions in perturbed nitroxides. *J. Amer. Chem. Soc.* **95**:2061

Daudel, R., Lefebvre, R., Moser, C. 1959. Quantum Chemistry, Methods and Applications. Wiley-Interscience, New York

Davson, H., Danielli, J. F. 1943. The Permeability of Natural Membranes. Cambridge University Press, New York

Eichberg, J., Whittaker, V. P., Dawson, R. M. C. 1964. Distribution of lipids in subcellular particles of guinea-pig brain. *Biochem. J.* **92**:91

Folch, J., Lees, M., Stanley, G. H. S. 1957. A simple method for the isolation and purification of total lipids from animal tissues. *J. Biol. Chem.* **226**:497

Griffith, O. H. 1965. ESR and electronic structure of the RĊHOR′ ether radicals. *J. Chem. Phys.* **42**:2651

Griffith, O. H., Libertini, L. J., Birrell, G. B. 1971. The role of lipid spin labels in membrane biophysics. *J. Phys. Chem.* **75**:3417

Hall, J. E., Meade, C. A., Szabo, G. 1973. A barrier model for current flow in lipid bilayer membranes. *J. Membrane Biol.* **11**:75

Hubbell, W. L., McConnell, H. M. 1968. Spin-label studies of the excitable membranes of nerve and muscle. *Proc. Nat. Acad. Sci.* **61**:12

Hubbell, W. L., McConnell, H. M. 1971. Molecular motion in spin-labeled phospholipids and membranes. *J. Amer. Chem. Soc.* **93**:314

Jost, P. C., Griffith, O. H., Capaldi, R. A., Vanderkooi, G. 1973. Evidence for boundary lipid in membranes. *Proc. Nat. Acad. Sci.* **70**:480

Jost, P., Libertini, L. J., Hebert, V. C., Griffith, O. H. 1971*a*. Lipid spin labels in lecithin multilayers. A study of motion along fatty acid chains. *J. Mol. Biol.* **59**:77

Jost, P., Waggoner, A. S., Griffith, O. H. 1971*b*. Spin labeling and membrane structure. *In:* The Structure and Function of Biological Membranes. L. I. Rothfield, editor. Ch. 3, p. 84. Academic Press Inc., New York

Kabankin, A. S., Zhidomirov, G. M., Buchachenko, A. L. 1973. Structure of complexes of radicals with organic ligands. *J. Magn. Reson.* **9**:199

Karplus, M., Fraenkel, G. K. 1961. Theoretical interpretation of carbon-13 hyperfine interactions in electron spin resonance spectra. *J. Chem. Phys.* **35**:1312

Kawamura, T., Matsunami, S., Yonezawa, T. 1967. Solvent effects on the *g*-value of di-*t*-butyl nitric oxide. *Bull. Chem. Soc. Japan* **40**:1111

Lajzerowicz-Bonneteau, J. 1968. Structure du radical nitroxide tetramethyl-2,2,6,6-piperidinol-4-oxyle-1. *Acta Cryst.* **B24**:196

Lemaire, H., Rassat, A. 1964. Structure hyperfine due a l'azote dans les radicaux nitroxydes. *J. Chim. Phys.* **61**:1580

Libertini, L. J., Griffith, O. H. 1970. Orientation dependence of the electron spin resonance spectrum of di-*t*-butyl nitroxide. *J. Chem. Phys.* **53**:1359

Libertini, L. J., Waggoner, A. S., Jost, P. C., Griffith, O. H. 1969. Orientation of lipid spin labels in lecithin multilayers. *Proc. Nat. Acad. Sci.* **64**:13

Lim, Y. Y., Drago, R. S. 1971. Donor properties of a free-radical base. *J. Amer. Chem. Soc.* **93**:891

McConnell, H. M., McFarland, B. G. 1972. The flexibility gradient in biological membranes. *Ann. N.Y. Acad. Sci.* **195**:207

Murata, Y., Mataga, N. 1971. ESR and optical studies on the EDA complexes of di-*t*-butyl N-oxide radical. *Bull. Chem. Soc. Japan* **44**:354

Mysels, K. J. 1959. Introduction to Colloid Chemistry. Ch. 15. Wiley-Interscience, New York

Neumcke, B., Läuger, P. 1969. Nonlinear electrical effects in lipid bilayer membranes. II. Integration of the generalized Nernst-Planck equations. *Biophys. J.* **9**:1160

Omura, T., Siekevitz, P., Palade, G. E. 1967. Turnover of constituents of the endoplasmic reticulum membranes of rat hepatocytes. *J. Biol. Chem.* **242**:2389

Onsager, L. 1936. Electric moments of molecules in liquids. *J. Amer. Chem. Soc.* **58**:1486

Pauling, L. 1960. The Nature of the Chemical Bond, Third Edition. p. 90. Cornell University Press, Ithaca, New York

Perrin, D. D. 1963. Buffers of low ionic strength for spectrophotometric pK determinations. *Aust. J. Chem.* **16**:572

Rottem, S., Hubbell, W. L., Hayflick, L., McConnell, H. M. 1970. Motion of fatty acid spin labels in the plasma membrane of mycoplasma. *Biochim. Biophys. Acta* **219**:104

Rozantsev, E. G. 1970. Free Nitroxyl Radicals. Plenum Press, New York

Rozantsev, E. G., Sholle, V. D. 1971. Progress in the chemistry of nitroxyl radicals. *Uspekhi Khimii* **40**:417. Eng. trans.: *Russ. Chem. Rev.* **40**:233

Seelig, J. 1970. Spin label studies of oriented smectic liquid crystals (A model system for bilayer membranes). *J. Amer. Chem. Soc.* **92**:3881

Seelig, J., Limacher, H., Bader, P. 1972. Molecular architecture of liquid crystalline bilayers. *J. Amer. Chem. Soc.* **94**:6364

Selinger, Z., Lapidot, Y. 1966. Synthesis of fatty acid anhydrides by reaction with dicyclohexylcarbodiimide. *J. Lipid Res.* **7**:174

Singer, S. J. 1971. The molecular organization of biological membranes. *In:* The Structure and Function of Biological Membranes. L. I. Rothfield, editor. Ch. 4, p. 146. Academic Press Inc., New York

Singer, S. J., Nicolson, G. L. 1972. The fluid mosaic model of the structure of cell membranes. *Science* **175**:720

Steck, T. L., Fairbanks, G. F., Wallach, D. F. H. 1971. Disposition of the major proteins in the isolated erythrocyte membrane. Proteolytic dissection. *Biochemistry* **10**:2617

Streitwieser, A. 1961. Molecular Orbital Theory. p. 47. John Wiley & Sons (Wiley-Interscience), New York

Sysoeva, N. A., Stepanyants, A. U., Buchachenko, A. L. 1968. Paramagnetic shift of solvent protons in the presence of organic radicals. *Z. Struk. Khimii* **9**:311. Eng. trans.: *J. Struct. Chem.* **9**:248

Thompson, T. E., Henn, F. A. 1970. Experimental phospholipid model membranes. *In:* Membranes of Mitochondria and Chloroplasts. E. Racker, editor. Ch. 1, p. 1. Van Nostrand Reinhold Co., New York

Vanderkooi, G., Green, D. W. 1971. New insights into biological membrane structure. *BioScience* **21**:409

Vasserman, A. M., Buchachenko, A. L. 1966. The EPR spectra and electronic structure of nitric oxide radicals. *Z. Struk. Khimii* **7**:673. Eng. trans.: *J. Struct. Chem.* **7**:633

Waggoner, A. S., Griffith, O. H., Christensen, C. R. 1967. Magnetic resonance of nitroxide probes in micelle-containing solutions. *Proc. Nat. Acad. Sci.* **57**:1198

Waggoner, A. S., Keith, A. D., Griffith, O. H. 1968. ESR of solubilized long-chain nitroxides. *J. Phys. Chem.* **72**:4129

Waggoner, A. S., Kingzett, T. J., Rottschaefer, S., Griffith, O. H., Keith, A. D. 1969. A spin-labeled lipid for probing biological membranes. *Chem. Phys. Lipids* **3**:245

Weast, R. C., editor. 1972. Handbook of Chemistry and Physics, 53rd Edition. The Chemical Rubber Co., Cleveland, Ohio

Wertz, J. E., Bolton, J. R. 1972. Electron Spin Resonance. p. 125. McGraw-Hill Book Co., Inc., New York